Solid-State Lamp with Integral Occupancy Sensor

John J. Cooley *Student Member, IEEE*, Dan Vickery, Al-Thaddeus Avestruz *Member, IEEE*,
Amy Englehart, James Paris, and Steven B. Leeb *Fellow, IEEE*

Abstract—**Previous work demonstrated a retrofit proximity detector for fluorescent lamps using the lamp's own stray electric fields. This paper extends the retrofit sensor system to a solid-state (LED) lamp. The design and implementation of a suitable driver ("ballast") for the LED lamp is presented. Design considerations for the ballast include those relevant to lighting (e.g. color cast and dimming levels) as well as those relevant to sensing of human occupants. Two electro-quasistatic modeling approaches for the lamp sensor are discussed. Experimental data from the LED lamp sensor are presented and compared to one of the proposed quasistatic models.**

I. INTRODUCTION: ENERGY EFFICIENT LIGHTING TECHNOLOGY

New illumination sources and new power electronic controls for lighting have the potential to produce energy efficiency gains of 240 percent in the residential sector and 150 percent in the commercial sector [1]. In 2007, lighting accounted for 15.6 percent and 23.3 percent of all electricity consumed in the residential and commercial sectors, respectively, in the USA, [1]. Efficiency gains from lighting sources and active control can substantially reduce overall energy consumption. In particular, solid-state lighting promises improved energy efficiency and long lifetime [2].

A fluorescent lamp with an integral occupancy sensor was demonstrated in [3], [4] and [5]. By exploiting the lamp's own stray electric field, the sensor system is able to detect changes in the electric field below the lamp. Unlike standard proximity sensors which require building planners to design for a proximity detection system separate from the lighting system, this proximity sensor is essentially a drop-in replacement for a standard commercial fluorescent lamp ballast.

This paper describes the extension of the lamp sensor to a solid-state (LED) lamp of similar construction to a fluorescent lamp. The design and implementation of a suitable driver ("ballast") for the LED lamp is presented here. Design considerations for the ballast include those relevant to lighting. For example, the ballast may be designed to achieve consistent color cast across dimming levels. The ballast must be designed to support the lamp sensor electronics by driving the lamp with an alternating voltage. An overview of the lamp sensor from [3]–[5], as well as two electro-quasistatic modeling approaches, are discussed in Section II. The design and implementation of the ballast for the LED lamp is discussed in Section III. Finally, experimental data from the lamp sensor built around the LED lamp are presented and compared to one of the proposed quasistatic models in Section IV.

II. LAMP SENSOR OPERATION AND MODELING

A. System description

The block diagram of the lamp sensor is shown in Figure 1. A suitable lamp and electrode arrangement is depicted in Figure 2. A typical fluorescent or LED lamp may include an electronic ballast that drives the bulbs with an alternating voltage at frequencies in the range of 20 to 50 kHz. As long as the lamp is driven with an alternating voltage, we have found that an electrostatic proximity sensor (lamp sensor) can be developed to measure the resulting stray electric fields below the lamp. In this section, we describe the operating principles of the lamp sensor that may be applied to either a fluorescent or LED lamp. Section III describes a driver specifically suited to operating LED lamps with the proximity detector.
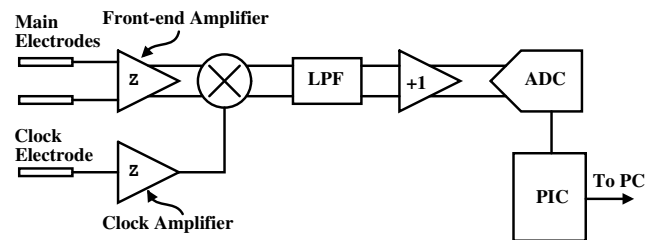

Fig. 1. The block diagram of the lamp sensor. Transimpedance amplifiers are marked with a 'Z'.
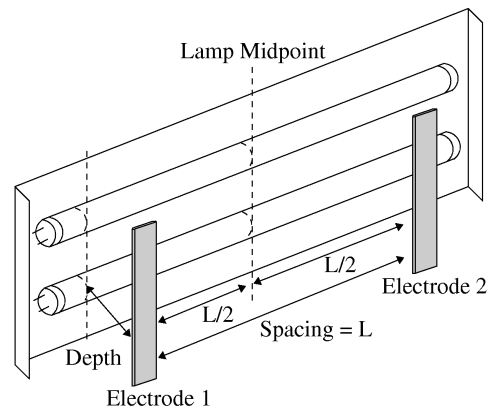

Fig. 2. A diagram of a typical two-bulb fluorescent lamp and electrode configuration. The electrodes are spaced symmetrically about the center of the lamp.

The lamp sensor measures low frequency ($\sim$0.1-5Hz) changes caused by human targets below the lamp in the high-frequency ($\sim$50kHz) alternating stray electric fields coupling

from the lamp. The lamp sensor measures the electric fields in front of the lamp with a fully-differential transimpedance front-end amplifier driven by the two electrodes depicted in Figure 2. The front-end amplifier is fully-differential because both its inputs and outputs are differential. When the electric fields measured by the two electrodes are equal, the differential measurement is balanced and the front-end output voltage is "nulled" to zero volts. Therefore, the front-end can have very high gain without saturating its output in the absence of a detection. This very high gain is necessary to amplify the effects of small imbalances in the capacitive system below the lamp. Furthermore, the fully-differential structure of the front-end amplifier relaxes the need for a specific ground reference in the lamp sensor system.

As indicated in Figure 1, the lamp sensor uses synchronous detection to reject stray signals that differ in phase or frequency from the lamp's own excitation signal. Synchronous detection is achieved with a separate measurement of the signal source. The lamp sensor system multiplies this reference signal with the main signal using a fully-differential multiplier. Whereas low-frequency occupant motion below the lamp naturally modulates the high-frequency signal measured by the front-end, the output of the multiplier (demodulator) contains the low-frequency modulations centered on zero frequency (dc). A low-pass filter (LPF) attenuates the high-frequency residue from the multiplier output to yield only the low-frequency signal. The synchronous detector and modulation-demodulation scheme also has the advantage of bypassing potentially overwhelming low-frequency 1/f noise in the front-end amplifier. Bypassing 1/f noise is critical because the signals of interest (occupancy detections) are very low in frequency. The signal of interest is amplified having been naturally up-modulated by the lamp sensor system to high-frequency (∼50kHz). The amplified high frequency signal is then downmodulated by the multiplier shown in Figure 1 after amplification. Meanwhile, the low-frequency 1/f noise generated within the front-end amplifier is up-modulated by the multiplier to high-frequency and attenuated by the ensuing LPF. This signal detection scheme is not unlike chopper stabilization of op-amps for elimination of low-frequency noise, detection in an AM radio, or the so-called "lock-in" amplification technique for frequency specificity. Note that this system comprises a suppressed-carrier AM modulation-demodulation signal chain. That is, when there is no detection, there is also no carrier signal measured by the sensor. This is fundamentally why a "clock electrode" (depicted in Figure 1) is necessary to obtain a phase and frequency reference for the desired signal.

Measurement of the electric field can be taken as a measurement of the two electrode potentials (at electrode 1 and electrode 2 in Figure 2) referenced to some arbitrary potential. This corresponds to a voltage-mode measurement and requires a high input impedance measurement device. Alternatively, the electric field measurement can be taken as a measurement of the current shunted between the electrodes when they are connected by a short-circuit. This corresponds to a current-

mode measurement and requires a low input impedance measurement device. In the lamp sensor, a fully-differential current-mode amplifier is used as the front end amplifier depicted in Figure 1. Reference [6] details the behavior and operating principles of fully-differential amplifiers like the one used here. In [5], we reported 11ft. of detection range between the lamp and the closest edge of a human target. For a detailed description of the lamp sensor operation, see references [4], [5].

B. Capacitive Modeling

The electric field measurement may be modeled as a measurement within a capacitive network. Such a capacitive network may be comprised of the capacitances connecting all of the conducting objects in the system. This abstraction is a starting point for qualitatively understanding the behavior of the lamp sensor system and its key features. Implicit in this abstraction is that the objects of interest can be represented by conducting surfaces. While some objects in the system are obviously well-represented as conducting surfaces (e.g. the electrodes), the fluorescent lamp bulbs as well as the human target are also represented this way. References [7]–[9] describe the implications of approximating a human as a conducting shell. Reference [5] motivates the treatment of the bulb surfaces as voltage or low-impedance sources rather than current or high-impedance sources in the capacitive system. Reference [10] discusses the approximation of lumping each of the bulbs into "positive" and "negative" source ends. Furthermore, the floor below the lamp is taken as a conducting plane and could be arbitrarily chosen as the potential reference (ground) for the system.

Having these assumptions, we can build a capacitive model like the one proposed in Figure 3 by accounting for capacitances between the conducting objects in the lamp sensor system. Accurate modeling of the lamp sensor system using this modeling approach typically requires the use of capacitance extraction software. Note that the capacitive model pictured in Figure 3 differs from the electrostatic model described and used in Section IV in at least one key way. Most notably, the low-potential source ends of the lumped signal sources in Figure 3 are not grounded as they are in the model described in Section IV.
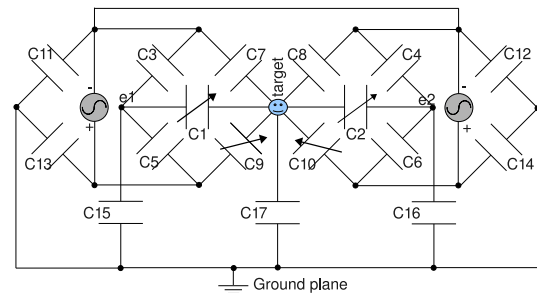

Fig. 3. Capacitive Model of fluorescent lamp sensor.

C. Quasi-Analytical Modeling

Another approach to modeling the lamp sensor system is to solve Laplace's equation, $\nabla^2 \Phi = 0$, directly for the potential everywhere in the system in order to get an equation for the electrode voltage. To that end, a reduced model of the lamp sensor may be developed by modeling the important conducting surfaces in the system as charged conducting spheres. An example of such a reduced model is shown in Figure 4. Modeling the conducting surfaces as conducting spheres is advantageous because the analytical expressions for the potential outside (and inside) a charged conducting sphere are readily available. Moreover, through linear superposition of potential (scalar) fields, the problem of determining the potential everywhere in a system with one sphere can be extended to the problem of determining the potential everywhere in a system with K spheres.

Fig. 5. Coordinate system of one sphere with radius a. r, θ and φ are standard spherical coordinates; that is, they are respectively, radius, pitch angle and azimuthal angle with the origin being the center of the sphere.
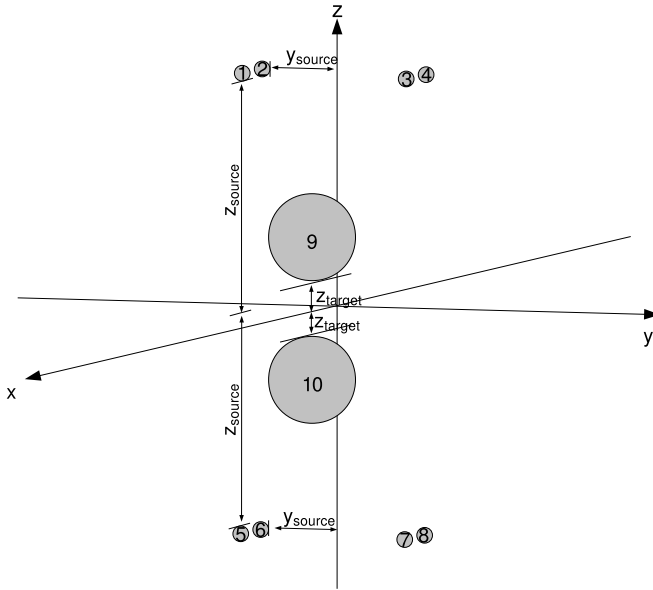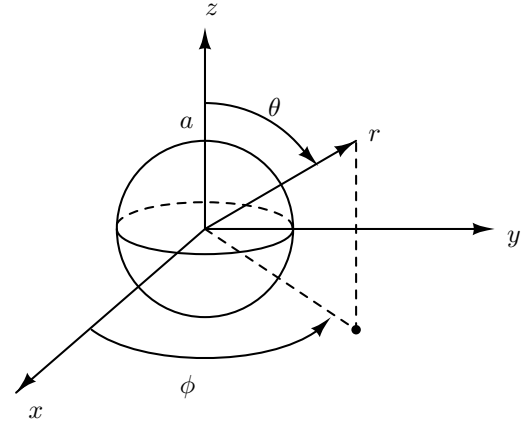

Fig. 4. Sphere model used to represent lamp sensor and target. Spheres 1, 2, 3 and 4 represent the signal sources created by the lamp. Sphere 9 represents the target. Modeling the floor as a conducting plane is achieved using the method of images, and hence spheres 5, 6, 7, 8 and 10.

D. Modeling one conducting sphere

For a charged sphere with radial boundary a as shown in Figure 5, the solution of the potential field everywhere outside the boundary a is well-known as the summation in (1). The summation contains Legendre polynomials, $P_n^m(x)$'s, where x is replaced by the pitch-angle function $\cos\theta$ as follows [11]–[14]:

$$\Phi(r,\theta,\varphi) = \sum_{n=0}^{R}\sum_{m=-n}^{n}\left(\frac{A_{nm}}{r^{n+1}}P_n^m(\cos\theta)e^{jm\varphi}\right), \quad (1)$$

For a single charged conducting sphere, equation (1) can be rewritten in vector form as

$$\Phi(r,\theta,\phi) = p^T\alpha, \quad (2)$$

where α is a vector containing the A_{nm} coefficients:

$$\alpha^T = (A_{00}, A_{1,-1}, A_{1,0}, A_{1,1}, A_{2,-2}, A_{2,-1}, ..., A_{R,R}) \quad (3)$$

The vector p contains the rest of each term in the summation of (1), so that the first few entries of p are

$$p_0 = \frac{1}{r}P_0^0(\cos\theta)$$

$$p_1 = \frac{1}{r^2}P_1^{-1}(\cos\theta)e^{-j\phi}$$

$$p_2 = \frac{1}{r^2}P_1^0(\cos\theta)$$

$$p_3 = \frac{1}{r^2}P_1^1(\cos\theta)e^{j\phi}$$

$$p_4 = \frac{1}{r^3}P_2^{-2}(\cos\theta)e^{-2j\phi}$$

$$\vdots$$

Taking the inner product of the vectors p and α above (as described by (2)) results in $\Phi(r,\theta,\phi)$ from (1). Having fixed the coordinate reference for (r,θ,ϕ), the Legendre polynomials, $P_n^m(\cos\theta)$, can be "looked up" to form the vector p. Then, the A_{nm} coefficients are unknowns that must be found before we can find the potential everywhere in the system, $\Phi(r,\theta,\phi)$. For a given order of the multipole expansion described by equation (1), we take N as the number of terms in the summation leaving us with as many unknown A_{nm} coefficients to find. To that end, $M > N$ independent equations can be formed by "sampling" the potentials at M points in the system leading, each one yielding an equation like the one in (1). The sampled potentials are known potentials, otherwise known as boundary conditions on the conducting surfaces in the system. The resulting M equations can be written in matrix form as follows:

$$b = \mathbf{P}\alpha, \quad (4)$$

where P is an $M \times N$ matrix, b is the vector containing the M potentials from the left side of (2):

$$b = \begin{bmatrix} \Phi(r_1, \theta_1, \varphi_1) \\ \Phi(r_2, \theta_2, \varphi_2) \\ . \\ . \\ . \\ \Phi(r_N, \theta_N, \varphi_N) \end{bmatrix} \quad (5)$$

and $\mathbf{P}$ is a matrix whose rows are the N transposed p vectors from the right side of (2):

$$\mathbf{P} = \begin{bmatrix} p_0^T \\ p_1^T \\ . \\ . \\ . \\ p_N^T \end{bmatrix} \quad (6)$$

Then, a least-squares formulation for the solution to α is:

$$\alpha = (\mathbf{P}^T \mathbf{P})^{-1} \mathbf{P}^T b \quad (7)$$

so that, upon substituting this result for α into (2), the value of the potential at (r, θ, ϕ) can be found directly as follows:

$$\boxed{\Phi(r, \theta, \phi) = p^T \left((\mathbf{P}^T \mathbf{P})^{-1} \mathbf{P}^T b \right)} \quad (8)$$

Having fixed the geometry of the system and the boundary values on the conducting surfaces by defining the p vectors in equation (6), and the values comprising the vector b in equation (5), as well as the order of the multipole expansion, one can directly compute the potential at any point (r, θ, ϕ) using equation (8). While the vector of A_{nm} coefficients given by equation (7) is valid for computing the potential from any equation of the form in (1), choosing the particular vector p effectively establishes the coordinate reference for (r, θ, ϕ) within the system by choosing one particular equation of the form in (2).

E. Modeling K Charged Conducting Spheres

The development above, for calculating the potential in a system with one charged sphere, can be extended to calculate the potential in a system with K spheres. The potential due to each sphere is summed as follows:

$$\Phi = \Phi_1 + \Phi_2 + ... + \Phi_k + ... + \Phi_K. \quad (9)$$

Each potential, Φ_k, is a summation like the one in (1). For each summation leading to Φ_k, the variables r_k, θ_k and φ_k are the standard spherical coordinates with their origin at the center of the kth sphere.

The total potential from (9) for the K sphere case can also be re-written in vector form in analogy to equation (2) as follows:

$$\Phi = p_1 \alpha_1 + p_2 \alpha_2 + ... + p_K \alpha_K \quad (10)$$

Now, the charge distribution on each sphere depends on the charge distribution on the other spheres. Therefore, in the calculation of each Φ_k for eqn. (10), we take into account

the boundary conditions on all K spheres by extending b to include the boundary conditions on all K spheres and $\mathbf{P}$ to include known position terms for all K spheres. Lastly α is extended to include unknown coefficients for all K spheres. The augmented matrices described above can be written in matrix equation form corresponding to the equation in (4) as follows:

$$\begin{bmatrix} b_1 \\ b_2 \\ . \\ . \\ . \\ b_K \end{bmatrix} = \begin{bmatrix} \mathbf{P_{11}} & \mathbf{P_{12}} & . & . & . & \mathbf{P_{1K}} \\ \mathbf{P_{21}} & \mathbf{P_{22}} & . & . & . & \mathbf{P_{2K}} \\ . & . & . & . & . & . \\ . & . & . & . & . & . \\ . & . & . & . & . & . \\ \mathbf{P_{K1}} & \mathbf{P_{K2}} & . & . & . & \mathbf{P_{KK}} \end{bmatrix} \begin{bmatrix} \alpha_1 \\ \alpha_2 \\ . \\ . \\ . \\ \alpha_K \end{bmatrix}, \quad (11)$$

where

$$b_m \in \mathbb{R}^{M \times 1} \quad (12)$$
$$\alpha_m \in \mathbb{R}^{N \times 1} \quad (13)$$
$$P_{mn} \in \mathbb{R}^{M \times N}. \quad (14)$$

Finally, in the K-sphere case, $\Phi(r, \theta, \phi)$ may be directly computed as in (8) by using the augmented vector b and matrix $\mathbf{P}$ shown in (11).

The analytical model above can be validated by comparison between analytical results and simulations from Maxwell 2D as in Figure 6. Figure 6 is a plot of the percent error between the two methods for the potential around a charged conducting sphere. The data for this case show that the magnitude of the error between the simulation and the analytical model is no larger than 0.5%. In Section IV, an analytical model of the lamp sensor system will be compared to measured results.
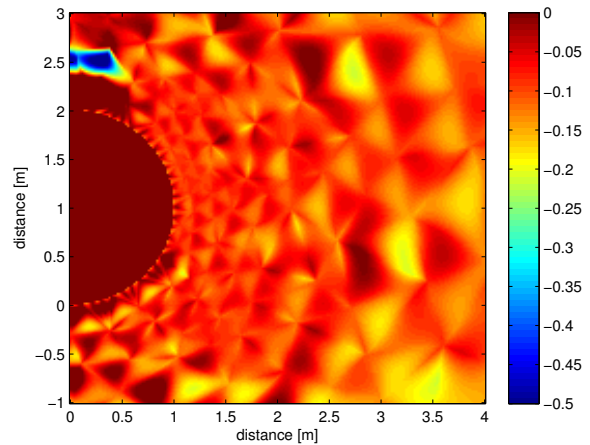

Fig. 6. The percent error between Maxwell 2D® results, Φ_{Mxwl}, and least-squares method results, Φ_{LstSq}. The conducting sphere has radius 1 m and a surface potential of 100 V referenced to the zero-potential at $r = \infty$

III. POWER ELECTRONIC LED DRIVE AND DIMMING

Power electronic drives represent a significant efficiency improvement over linear power sources. In LEDs, light output is best controlled by regulating current. Some difficulties in

using the terminal voltage as the control include a negative temperature coefficient that leads to thermal runaway and a poorly behaved exponential relation to power output.

The salient characteristic of a linear regulator is that a voltage is dropped across an element that continuously carries current, resulting in an inescapable power dissipation. Linear current regulators can use active devices in either open-loop (e.g. current mirror) or closed loop (e.g. op-amp with a pass transistor). A voltage source with a series resistor is also used in driving LEDs-the underlying approximation is that the voltage drop across the resistor is large, hence approximating a current source, which means that it is guaranteed that power is dissipated as heat by the resistor. This approximation weakens at low current levels when dimming, resulting in a drifting current level and hence light output.

Pulse width modulation of the current is an effective approach to driving an LED. Not only is there an advantage in efficiency, but a number of studies have suggested that there may be an advantage to the quality of lighting [15], [16]. There are a number of choices for the design of a switching current source. Our design was based on several requirements, which include a bipolar source for proximity sensing, square current pulses for color quality, and a wide dimming range.

A. Power Circuit Implementation

We chose a buck converter with a hysteretic current controller and a post-inverter. The circuit is designed to operate from a 170 V dc bus (nominal rectified line voltage) driving two parallel strings of 40 mA ac LED modules, which are illustrated in Figure 7. Currently, we use commercially available modules with 14 LEDs in a diode bridge. These modules are meant to be used in low-voltage 60 Hz sockets meant for halogen lighting and hence a diode bridge with slow recovery. The problems with the reverse recovery when using a high frequency inverter were avoided by using a fast recovery bridge. The partitioning of these LEDs into bridged segments in these commercial modules are by no means optimal from the perspective of cost, power efficiency, and lamps sensor operation, but represent a good proof-of-principle. A future implementation will optimize a taper in the partitioning of LEDs into bridged segments with an electric field distribution that is suitable for the lamp sensor, while minimizing the number of necessary diode bridges.

A schematic of the power system is shown in Figure 8. The buck converter was designed to switch at hundreds of kilohertz, while the inverter was designed to operate in the 20–30 kHz range. Because the full-bridge inverter is driven by a current source with free-wheel diode, D_2, no dead-time circuitry for the switches is necessary, which simplifies the design. Transformer T_1 is a $1:1$ isolation transformer that allows an electrical configuration, where the opposing corner terminals are nominally at the same potential as the floor and fixture, which may result in an improved sensitivity in the lamp sensor. Transformer T_2 is a small current balancing transformer, similar to those which are used in fluorescent lamp ballast. The volt-second demands on this transformer
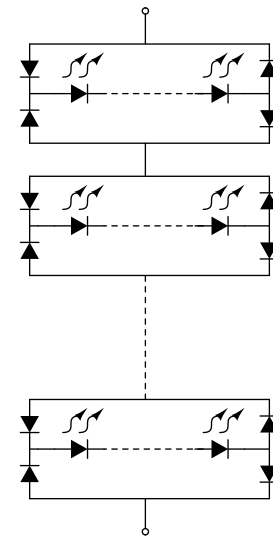

Fig. 7.   Bidirectional LED modules.

are small because they corresponds to the average ensemble mismatch among LEDs in each string.
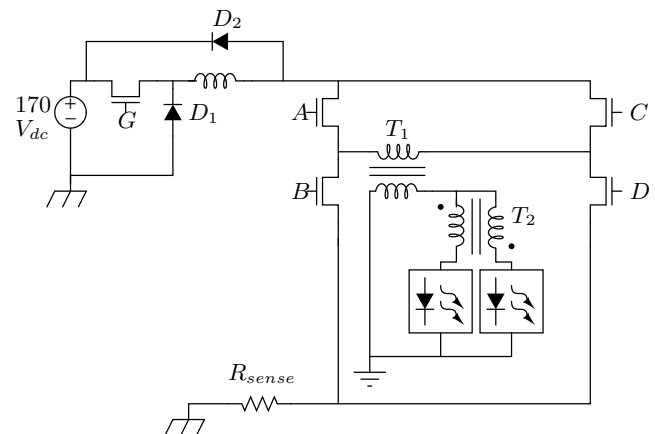

Fig. 8.   Schematic of the bipolar LED driver. Transformer T_1 isolates the inverter output. Transformer T_2 matches the currents between the two LED bulbs.

The buck converter controller shown in Figure 9 was set for a nominal current ripple of 10%. The inverter switches (A,B,C,D) and the gate drive enable (G_{EN}) are controlled by a DSPIC33FJ2560GP710 microcontroller with a fast PLD to create the inverter switching patterns.

Dimming is performed by symmetric tri-state PWM at the inverter. At high duty cycles ($> 60\%$), the buck converter is run at continuous current ($G_{EN} = 1$ always). This means that during the tri-state, we let the buck converter regulate the current into a short, i.e. either A and B ON, or C and D ON, and the complementary switches off. Table I shows inverter switching pattern for $D > 60\%$. CLK corresponds to an internal clock that determines the polarity of the inverter current and PWM is an internal state which corresponds to either the tri-state (LOGIC 0) or on-state (LOGIC 1). Figure
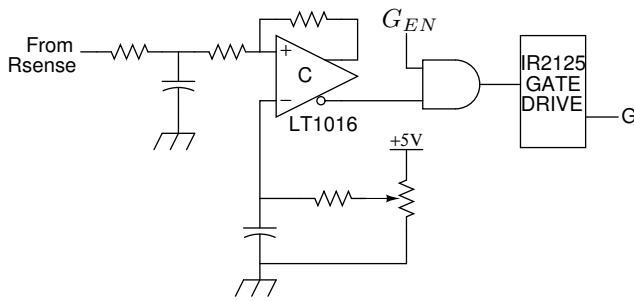
Fig. 9.   Hysteretic Current Controller.

CLK	PWM	A	B	C	D	G_{EN}	Status
1	0	0	0	0	0	0	LED OFF
1	0	1	1	0	0	1	Pre-Charge
1	1	1	0	0	1	1	LED POS Current
1	0	0	0	0	0	0	LED OFF/Discharge
0	0	0	0	0	0	0	LED OFF
0	0	0	0	1	1	1	Pre-Charge
0	1	0	1	1	0	1	LED NEG Current
0	0	0	0	0	0	0	LED OFF/Discharge

TABLE II
SWITCHING LOGIC PATTERN FOR LOW DUTY CYCLES WITH PRE-CHARGE.

CLK	PWM	A	B	C	D	Status
1	0	1	1	0	0	LED OFF
1	1	1	0	0	1	LED POS Current
1	0	0	0	1	1	LED OFF
0	0	0	0	1	1	LED OFF
0	1	0	1	1	0	LED NEG Current
0	0	1	1	0	0	LED OFF

TABLE I
SWITCHING LOGIC PATTERN WITH NO PRE-CHARGE. BUCK CONVERTER IS ALWAYS ENABLED.

10 illustrates the results at 96% inverter duty-cycle. *End-to-End Lamp Voltage* is the differential voltage across a single LED string. *LED Current* corresponds to the primary current of T_1 and closely represents the sum of the currents into the two parallel LED strings. A filtered version of *Clock*, with the spikes from switching transient pickup eliminated, is used for synchronization by the lamp sensor.
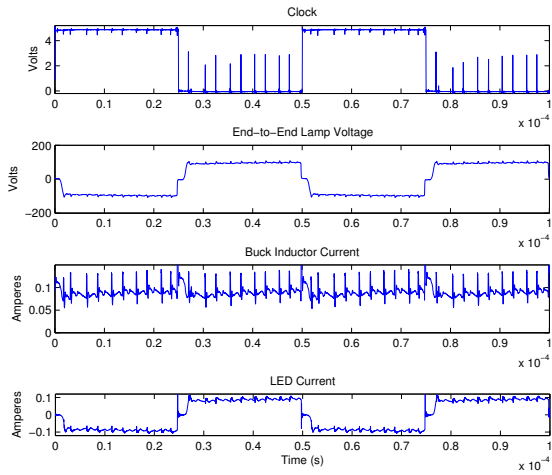
converter regulate and turning either A and B ON, or C and D ON, with the complementary switches off. Shorting the output of the buck converter in this way results in the fastest precharge for a given input voltage. Table II and the timing diagram in Figure 11 shows the switching pattern when inductor current pre-charging is used. By turning off the buck converter and recovering the inductor current, conduction losses are reduced for low duty ratios ($D < 60\%$). Pre-charging has the advantage of allowing a square LED current without needing very large inductor di/dt, obviating the need for small inductors at a very high switching frequency and the associated switching losses. The pre-charge time can be pre-determined by the rise time, $T_{rise} = LI_{pk}/V_{in}$, where L is a conservative estimate of the inductor value for all operating points and V_{in} is the input dc voltage to the buck converter, which could either be measured by the microcontroller, or set for worst-case low line voltage. Figure 12 shows the low-duty cycle waveforms with pre-charging.
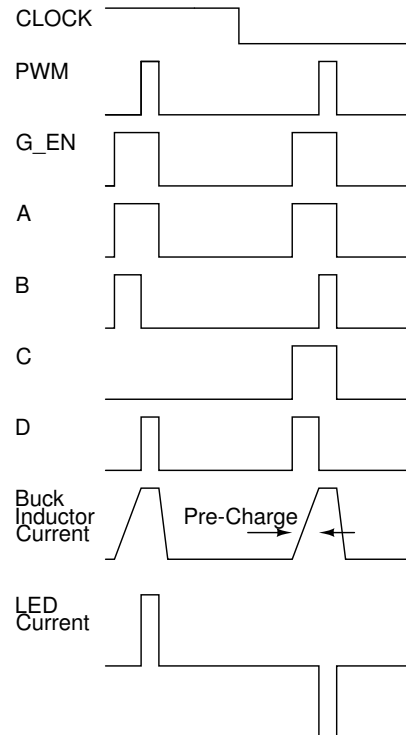

Fig. 10.   Waveforms at 96% Duty-Cycle with Continuous Inductor Current.

At low duty cycles ($< 60\%$), during the tri-state, we turn the buck converter off by gating switch G_{EN} off along with the inverter switches (A–D). This turns diodes D1 and D2 ON, hence recovering the inductor current. Prior to inverter current turn-on, we pre-charge the inductor by letting the buck
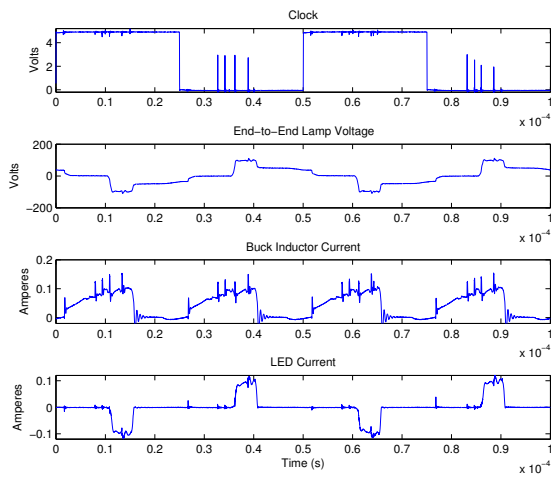

Fig. 11.   Timing Diagram Using Pre-Charging.

2310

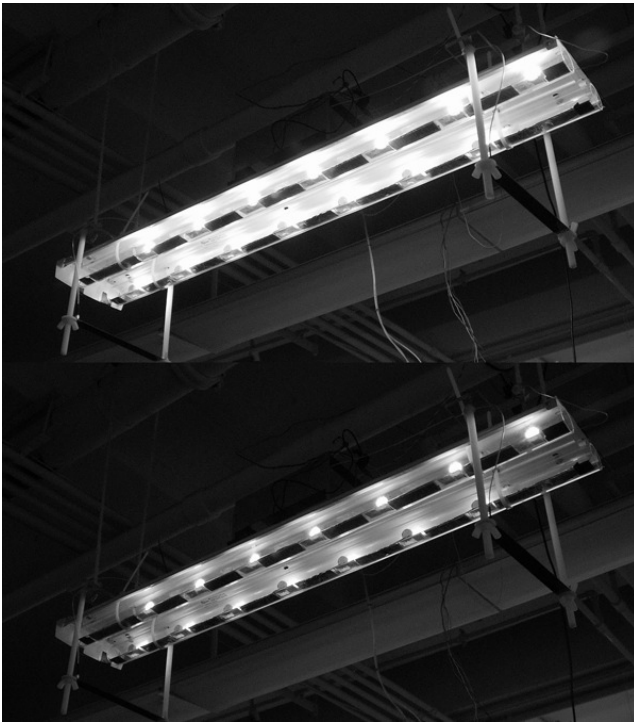Fig. 12. Waveforms at 10% Duty-Cycle with Inductor Current Pre-Charge.

Fig. 13. A photograph of the LED lamp. Top: bright, Bottom: dim.

IV. EXPERIMENTAL SETUP AND RESULTS

The experimental setup of the LED lamp and lamp sensor electronics is shown in Figure 14. The lamp sensor output was measured as a conducting sphere (the target) was passed under the lamp. Data was taken with the target fixed at 20 cm intervals in the y-dimension as depicted in Figure 14. For each interval, the lamp sensor output data was averaged for 20 seconds. The experiment was iterated for three lamp power settings "bright" (Duty ratio of 96%), "medium" (Duty

ratio of 60%)", and "dim" (Duty ratio of 20%). A photograph of the lamp under the "bright" and "dim" settings is shown in Figure 13. The experiment was also repeated for three x-displacements: 0 cm, 22 cm, and 45 cm.

The analytical approach described in Section II-C was also used to model the lamp sensor system. The electrostatic model of the lamp sensor consisted of conducting spheres representing the source nodes, electrodes and the target. The calculated difference between the electrode potentials was taken to be proportional to the output of the lamp sensor. Also, the floor was taken to be a conductor, so the model also consisted of image spheres below the plane of the floor. Finally, the potential of the "Lo" source nodes and of the plane of the floor was assumed to be earth ground.

To compare the analytical approach to measured data, the signal source parameters used in the electrostatic model were first calibrated. A "training run" consisted of taking measured data from the lamp sensor for known x and y displacements. Then, an iterative least-squares optimization method was used to infer the effective signal source parameters based on the measured data.

In the least-squares optimization method, the signal source parameters were first guessed. Then, the results of predicting the lamp sensor output using the electrostatic modeling approach from Section II-C and the guessed signal source parameters were compared to the measured data. Depending on the squared error between the predicted and measured data, the signal source parameters were perturbed and the process was repeated. This iterative process continued until the squared error between the predicted and measured lamp sensor output were less than a certain threshold. The signal source parameters from the last iteration were then taken as the actual effective signal source parameters in the lamp sensor system.

The measured and fitted data in Figure 15 correspond to training runs for each of the three lamp power settings. For each lamp power setting, we have different effective signal source parameters. Those effective signal source parameters were used to predict the lamp sensor response for different x-displacements. Figures 16(a), 16(b), and 16(c) compare those predictions to measured lamp sensor data at x-displacements of 22 cm and 45 cm for each of the three lamp power settings (dim, medium, and bright). The results in Figure 16 show that the modeling approach described in Section II-C yields predictive power for design-oriented estimation of the lamp sensor output voltage in response to a target.

V. CONCLUSION

Reference [17] is one of many references that discusses curtailed demand and its value in the energy market. In curtailed demand, the supply company reduces the effective energy demand by reclaiming unused or wasted energy. Reference [17] cites the sophisticated planning and knowledge of building characteristics necessary to implement curtailed demand and suggests that it can only be effective if "sensing and switching can be done cheaply" and with "a high level of automation."
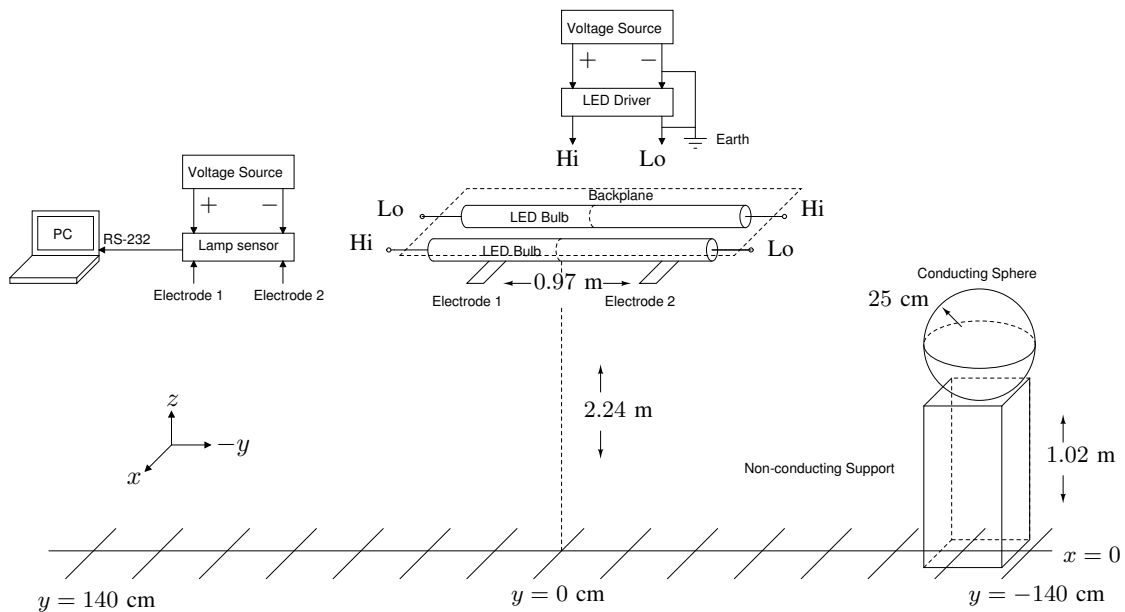
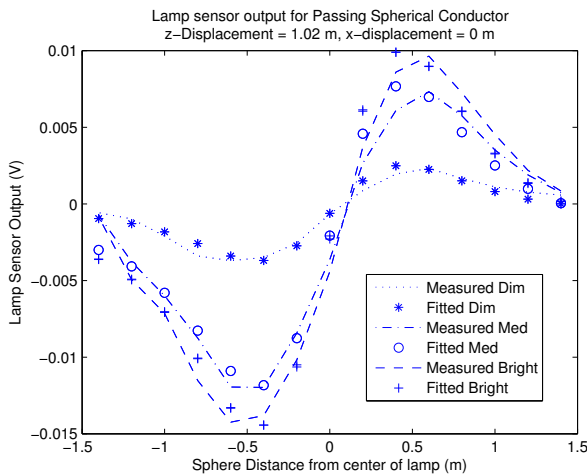Fig. 14.   The experimental setup.

Fig. 15.   Training runs (source calibration) $x = 0$ cm

important environmental variables such as time of day, through the actions of an embedded controller. The proximity sensor does not require motion or other intrusive occupant behavior to function. It is sensitive directly to the dielectric presence of an occupant. Interfacing the lamp sensor with a dimming ballast creates a smart auto-dimming lamp that can use the lamp sensor's occupancy detections to appropriately dim or brighten.

This paper has also demonstrated an electro-quasistatic model that accurately predicts the behavior of the proximity sensor for both fluorescent and solid state lamps. The model can be used by building designers to predict detection range given a particular configuration of luminaire. It can also be used to select a luminaire design to achieve needed detection range.

The incorporation of automatic proximity detection in solid state lighting could be a "game changing" addition to solid-state lamps that accelerates their acceptance.

Acknowledgments

In particular, there is a great interest in controlling lighting to optimize energy consumption. Lighting in commercial and residential spaces consumes a significant portion of the end use demand for delivered energy in the United States. In 2005, lighting consumed 0.73 Quadrillion Btu (QBtu) in the residential sector and 1.18 QBtu in the commercial sector [18].

This paper has presented a ballast or solid-state lamp driver that is suitable for dimmable operation of solid-state or LED lighting. The ballast described in this paper also creates the correct lamp current waveforms to permit a solid-state lamp to function effectively as a proximity sensor for occupants. This opens the door to distributed, autonomous control for lighting. That is, light fixtures can automatically alter their illumination based on the presence or absence of occupants, and any other

REFERENCES

[1] "Annual energy outlook 2009," Energy Information Administration: United States Department of Energy, March 2009.
[2] D. Steigerwald, J. Bhat, D. Collins, R. Fletcher, M. Holcomb, M. Ludowise, P. Martin, and S. Rudaz, "Illumination with solid state lighting technology," *Selected Topics in Quantum Electronics, IEEE Journal of*, vol. 8, no. 2, pp. 310–320, Mar/Apr 2002.

[3] J. J. Cooley, A.-T. Avestruz, S. B. Leeb, and L. K. Norford, "A fluorescent lamp with integral proximity sensor for building energy management," in *Power Electronics Specialists Conference, 2007. PESC 2007. IEEE*, June 2007, pp. 1157–1163.

[4] J. J. Cooley, A.-T. Avestruz, and S. B. Leeb, "An autonomous distributed demand-side energy management network using fluorescent lamp sensors," in *Power Electronics Specialists Conference, 2008. PESC 2008. IEEE*, June 2008.

[5] J. J. Cooley, "Capacitive sensing with a fluorescent lamp," Master's thesis, Massachusetts Institute of Technology, Cambridge, Massachusetts, 2007.

[6] J. J. Cooley, A.-T. Avestruz, and S. B. Leeb, "A design-oriented analytical approach for fully-differential closed-loop op-amp circuits."

[7] W. Buller and B. Wilson, "Measuring the capacitance of electrical wiring and humans for proximity sensing with existing electrical infrastructure," *Electro/information Technology, 2006 International Conference on*, pp. 93–96, 2006.

[8] P. Shahidi, A.V.; Savard, "A volume conductor model of the human thorax for field calculations," in *Proceedings of the Twelfth Annual International Conference of the IEEE*. Engineering in Medicine and Biology Society, November 1990, pp. 615–616.

[9] J. R. Smith, "Electric field imaging," Ph. D. Thesis, Massachusetts Institute of Technology, 1999.

[10] J. J. Cooley, "Capacitive sensing with a fluorescent lamp and applications."

[11] J. A. Stratton, *Electromagnetic theory*. McGraw-Hill book company, 1941.

[12] R. M. Fano, L. J. Chu, and R. B. Adler, *Electromagnetic fields, Energy and forces*. John Wiley and Sons, Inc., 1963.

[13] M. Zahn, *Electromagnetic Field Theory: a problem solving approach*. Krieger Publishing Company, 2003.

[14] J. D. Jackson, *Classical electrodynamics*. Wiley, 1999.

[15] M. Dyble, N. Narendran, A. Bierman, and T. Klein, "Impact of dimming white leds: Chromacity shifts due to different dimming methods," in *Fifth International Conference on Solid State Lighting, Proceedings of SPIE 5941*. Bellingham, WA: International Society of Optical Engineers, 2005, pp. 291–299.

[16] Y. Gu, N. Narendran, T. Dong, and H. Wu, "Spectral and luminous efficacy change of high-power leds under different dimming methods," in *Sixth International Conference on Solid State Lighting, Proceedings of SPIE 6337, 63370J*, 2006.

[17] K. Taylor, J. Ward, V. Gerasimov, and G. James, "Sensor/actuator networks supporting agents for distributed energy management," in *29th Annual IEEE International Conference on Local Computer Networks*, Bellingham, WA, November 2004, pp. 463 – 470.

[18] "Annual energy outlook 2007," Energy Information Administration: United States Department of Energy, February 2007.
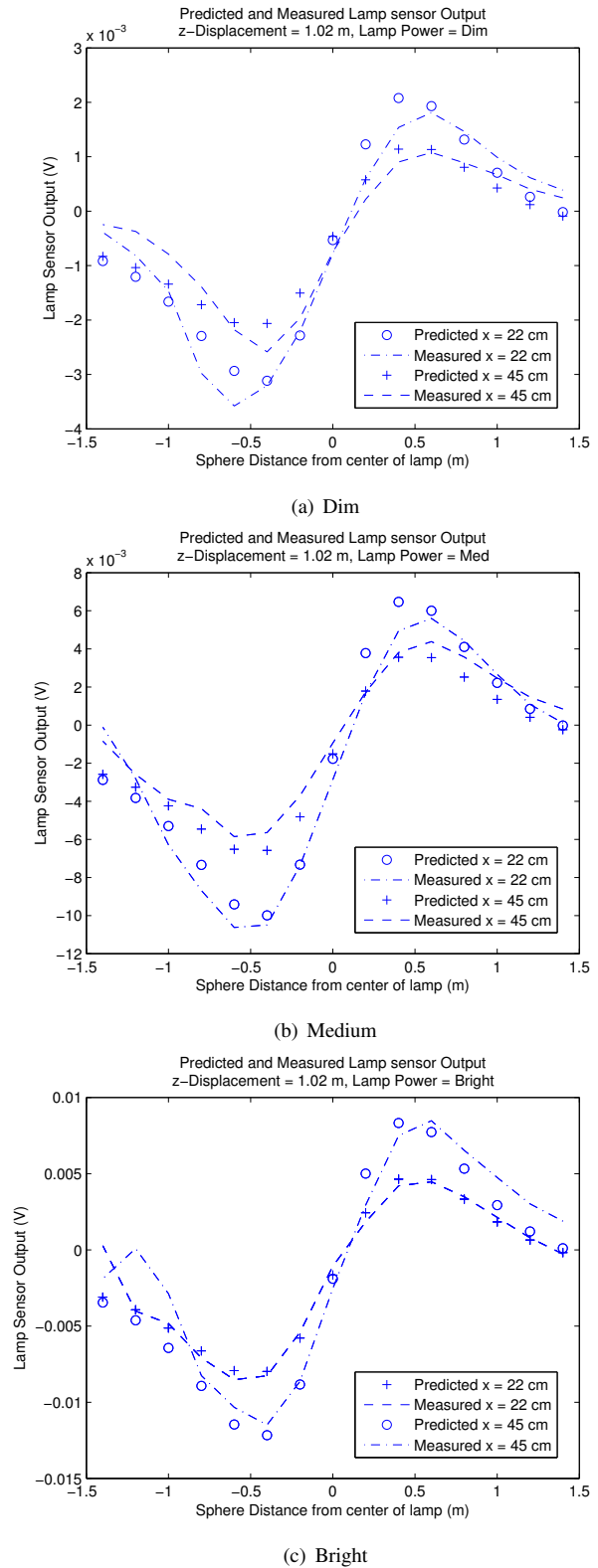
(a) Dim

(b) Medium

(c) Bright

Fig. 16. LED lamp sensor measured and predicted responses.